



# The circ\_006573/miR-376b-3p Axis Advances Spinal Cord Functional Recovery after Injury by Modulating Vascular Regeneration

Kun Wang<sup>1</sup> · Xinjin Su<sup>1</sup> · Qingxin Song<sup>1</sup> · Zhi Chen<sup>1</sup> · Hao Chen<sup>1</sup> · Yingchao Han<sup>1</sup> · Chao Zhu<sup>1</sup> · Hongxing Shen<sup>1</sup>

Received: 11 August 2022 / Accepted: 18 April 2023

© The Author(s), under exclusive licence to Springer Science+Business Media, LLC, part of Springer Nature 2023

## Abstract

Abnormal expression of non-coding RNAs after spinal cord injury (SCI) is associated with pathophysiological outcomes. We bioinformatically predicted a circRNA-miRNA-mRNA axis in SCI. A total of 4690 mRNAs, 17 miRNAs, and 3928 circRNAs were differentially expressed, with co-expressed RNAs predicted to regulate pathways related to wound healing. Among the most highly differentially expressed circRNAs, circ\_006573, but not circ\_016395, weakened the viability and migration of rat aortic endothelial cells, and its biological effects were rescued with miR-376b-3p mimics. Furthermore, circ\_006573 overexpression induced changes in Cebpb, IL-18, and Plscr1 expression that were reversed by miR-376b-3p. In a rat model, circ\_006573 shRNA administration improved the pathological manifestations of SCI and ameliorated motor function. Moreover, the expression of CD31, CD34, and VEGF-A in spinal cord tissues was significantly elevated after circ\_006573 shRNA treatment, indicating that circ\_006573 may be involved in vascular regeneration and functional recovery after SCI. Thus, the circ\_006573-miR-376b-3p axis offers a foundation for understanding pathophysiological mechanisms and predicting strategies for treating SCI.

**Keywords** spinal cord injury · circ\_006573 · miR-376b-3p · Anxa1 · rat aortic endothelial cells · angiogenesis

## Introduction

Spinal cord injury (SCI) is a central nervous system disease with high disability and mortality [1]. SCI may lead to the loss of sensory, motor, and autonomic functions below the injured segment [2]. With the increasing role of the transportation and construction industry in the modern social economy, the incidence rate of SCI is rising each year, thus posing a heavy burden to the patient's family and society [3]. Between 236 and 4187 people per million have experienced SCI [4], and the estimated global rate of SCI is between 250,000 and 500,000 new cases each year [5]. According

to the pathophysiology and development, SCI is usually divided into primary and secondary injury [6]. In the primary injury stage, physical tension causes cells in the damaged site to appear disintegrated, with signs of necrosis and apoptosis, as well as blood vessel rupture and tissue edema [7]. In the secondary injury stage, a large number of T cells, macrophages, microglia, and neutrophils infiltrate, thus damaging the blood-spinal cord barrier, releasing inflammatory factors, triggering a series of inflammatory cascade effects, and leading to secondary tissue injury [8]. Secondary injury may further affect the remodeling of synapses and regeneration of neural circuits, which may lead to permanent damage. Therefore, secondary injury is a major determinant of poor prognosis for SCI patients.

The nervous system is delicately coordinated by networks of genes, and SCI may severely damage its finely balanced regulation [9]. Accordingly, the treatment of SCI is a focus of research in the field of nerve injury regeneration [10]. Nerve cell regeneration, angiogenesis, anti-apoptosis, and anti-inflammatory processes affect the outcome of SCI [11]. SCI can cause immediate destruction of the nerve tissue, with direct vessel damage causing neuronal death [12], while angiogenesis is considered as

Kun Wang, Xinjin Su and Qingxin Song contributed equally to this work.

✉ Chao Zhu  
zhuchaode@gmail.com

✉ Hongxing Shen  
shenhxch@163.com; shenhongxing@renji.com

<sup>1</sup> Department of Spine Surgery, Department of Orthopedics, Renji Hospital, School of Medicine, Shanghai Jiao Tong University, Shanghai, China

a critical mechanism of spinal cord repair that stably supplies nutrients and oxygen to the injured site [13]. Insufficiency of the vascular network in the injury epicenter exacerbates the ischemia and apoptosis of nerve tissue [14]. Furthermore, angiogenesis has been shown to ameliorate neurobehavioral recovery after SCI [15, 16]. In a clinical assessment of SCI, intrathecal anti-Nogo-A antibody therapy ameliorated vascular germination and repair, and mitigated neurological deficits [17, 18]. Therefore, angiogenesis is a crucial function in the recovery of neurological functions after SCI.

In past decades, researchers have discovered that non-coding RNAs (ncRNAs) exert a crucial role in the progress of SCI [19, 20]. Various types of ncRNAs, including miRNAs, lncRNAs, and circRNAs, are associated with the initiation and development of SCI [21–23]. MiRNAs are involved in post-transcriptional regulation of gene expression; while circRNAs, which are synthesized by reverse splicing of coding RNAs or ncRNAs, have also emerged as having important roles in cancer biology [24]. Recently, circRNAs have suggested to have roles in both peripheral nerve injury and SCI [25]. Zhou et al. reported that differentially expressed circRNAs are involved in the pathogenesis of sciatic nerve injury and can be used as potential targets for the treatment [26]. Additionally, after SCI, a large number of circRNAs are differentially expressed, and some, such as circRNA\_07079 and circRNA\_01282, have been directly associated with SCI [27, 28]. Notably, circRNA expression in human cells is tissue-specific and demonstrates spatio-temporal specificity, with the circRNAs acting as miRNA sponges and blocking the downstream regulation of cell proliferation, metabolism, and metastasis by miRNAs [29]. Studies have increasingly shown that lncRNAs, miRNAs, and circRNAs form a complex regulatory network in cancer cells in which they act as competitive endogenous RNAs (ceRNAs) [30, 31]. In addition, it has been reported that circRNAs are expressed in coronary and brain aortic endothelial cells and have corresponding biological functions [32–34]. However, the role of the circRNA-miRNA-mRNA axis in angiogenesis of spinal cord after SCI is still lacking systematic research. Elucidating the expression pattern and function of specific ncRNAs may provide new biomarkers and new treatment strategies for SCI.

Herein, we systematically identified differentially expressed mRNAs, miRNAs, and circRNAs in SCI using high-throughput methods. We performed a series of functional and mechanistic assays showing that circ\_006573 has a core regulatory role in SCI. These assays were carried out using rat aortic vascular endothelial cells (RAOEC) and SCI model animals, thus laying a theoretical foundation for the clinical diagnosis and treatment of SCI

## Materials and Methods

### Acquisition and Screening of SCI-related Differentially Expressed circRNAs, miRNAs and mRNAs from Microarray Data

The sequencing datasets for this study were obtained from the Gene Expression Integration (GEO) database (<https://www.ncbi.nlm.nih.gov/GEO/>) [35] and included mRNA expression profiles from GSE45006 (4 SCI rats and 4 sham samples) and GSE52763 (8 SCI rats and 3 sham samples), miRNA expression profiles from GSE19890 (5 SCI rats and 5 sham samples), and circRNA expression profiles from GSE114426 (3 SCI rats and 3 sham samples).

Abnormally expressed genes were analyzed and screened using R software with the limma package [36]. The screening criteria were  $|\log \text{FC}| > 1.5$  and  $P < 0.05$ . GraphPad Prism 5 was used to draw volcano maps. The intersection of differentially expressed mRNAs in GSE45006 and GSE52763 chips was selected as the final screened differentially expressed mRNAs.

### Construction of SCI-related circRNA-miRNA-mRNA Interaction and Protein-protein Interaction Diagrams and Functional Enrichment Analysis

MiRanda database (<http://www.miranda.org/>), miRDB database (<http://mirdb.org/>) and miRTarBase (<http://mirtarbase.mbc.nctu.edu.tw>) were used to screen for co-expressed differentially expressed miRNAs, mRNAs and circRNAs. According to miRNA-mRNA and miRNA-circRNA relationship pairs, we used Cytoscape software (version 3.6.1) to construct and visualize ceRNA regulatory networks of circRNA-miRNA-mRNA [37]. The network diagram intuitively expresses interactions through nodes and wires, where each node represents a different RNA molecule and wires represent the interaction between nodes. Protein interaction analysis of the predicted target genes was performed using the online tool STRING (<https://string-db.org/>) [38]. The MCODE plug-in in Cytoscape was used to build protein-protein interaction networks.

To evaluate the potential functions of RNA molecules in the co-expression networks, Gene Ontology (GO) and KEGG analyses were performed using the Cytoscape plug-in ClueGO (<http://apps.cytoscape.org/apps/cluego>). Co-expressed mRNAs (39 in total) were used for enrichment analysis to infer the function of the co-expressed circRNAs. GO analysis included biological process (BP), molecular function (MF), and cellular component (CC) categories.

## Cell Culture and Transfection

RAOEC cells were acquired from WHELAB (Shanghai, China) and cultured in DMEM complete medium (M0101A, WHELAB) in an incubator (BB150, Thermo Fisher, USA). Plasmids for circ\_006573 and circ\_016395 overexpression were generated in pcDNA3.1 vector (V87020, Invitrogen, USA). MiR-376b-3p mimics (miR10003196-1-5) were purchased from RiboBio (China). Empty vector was used as a negative control (NC). RAOEC cells were transfected using Lipofectamine 3000 (L3000015, Invitrogen, USA). After 24–48 h, qRT-PCR was performed to assess transfection efficiency and biological function.

To evaluate the effects of circ\_006573 or circ\_016395, RAOEC cells were transfected with empty vector (NC group), circ\_006573 overexpression (circ\_006573-OE group), or circ\_016395 overexpression plasmid (circ\_016395-OE group); as well as with miR-376b-3p mimics (miR-376b-3p mimics group) or circ\_006573 overexpression plus miR-376b-3p mimics (circ\_006573-OE + miR-376b-3p mimics group).

## QRT-PCR Assays

Total RNA from RAOEC cells was isolated using the Total RNA Extractor kit (B511311, Sangon, China), followed by reverse transcription using a universal reverse transcription kit (AT341, TransGen, China). QRT-PCR was performed using SG Fast qPCR Master Mix (B639273, Sangon, China) in a PCR system (EDC-810, Eastwin Life Sciences, Inc.). Gene expression was calculated by the  $2^{-\Delta\Delta CT}$  method.

## Verification of circRNA Structure and Stability

To verify the circular structure of circ\_006573 and circ\_016395, total RNA was incubated with or without 3 U/ $\mu$ g RNase R (RNA07250, Epicenter, USA) for 60 min at 37°C. Then, qRT-PCR assays were performed to examine the levels of circ\_006573, circ\_016395, and GAPDH. The presence of circRNA as cDNA, rather than gDNA, was verified using convergent and divergent primers. The following thermocycling conditions were used: Initial denaturation at

95°C for 3 min, then 95°C for 7 sec, 57°C for 10 sec, and 72°C for 15 sec for 45 cycles. The primers used in this study are shown in Table 1.

## Cell Viability Assays

The cell counting kit-8 (CCK-8, E606335-0500, BBI Life Sciences, USA) was used to assess the proliferation of RAOEC cells. Cells ( $2 \times 10^4$  per well) were transfected with overexpression plasmids or mimics. After 24 hours, 10  $\mu$ L CCK-8 solution was added, and the cells were incubated for an additional 1 h. Finally, the absorbance (450 nm) of each well was assessed with a microplate reader (EPOCH2, Biotek, USA).

## Apoptosis Assays

RAOEC cell apoptosis was estimated using the Annexin V-FITC kit (556547, BD Pharmingen, USA). Transfected cells ( $1.5 \times 10^6$  per well) were harvested for 24 h, washed and centrifuged. A total of  $1.2 \times 10^6$  cells were resuspended in 100  $\mu$ L 1X binding buffer plus 5  $\mu$ L Annexin V-FITC. After incubation at 37°C in darkness for 10 min, 5  $\mu$ L propidium iodide (PI) was added to each well, and the plates were placed at 37°C in darkness for an additional 5 min. The percent apoptosis for each well was determined by flow cytometry (CytoFLEX, Beckman Coulter, USA).

## Cell Cycle Assays

The cell cycle distribution was evaluated using a Cell Cycle kit (C1052, Beyotime, China) according to the product manual. Briefly, RAOEC cells ( $2 \times 10^4$  per well) treated with trypsin washed with PBS and centrifuged at 1000 g for 4 min. Then, the cell pellets were fixed with 1 mL pre-cooled 70% ethanol at 4°C for 2 h. The cells were washed, and 0.5 mL PI staining solution was added to each sample in a dark room at 37°C for 30 min. Finally, the samples were examined by flow cytometry at an excitation wavelength of 488 nm.

**Table 1** Primer Information

Primer Information	Primer sequence (5'→3')	Amplification products (Bp)
h-GAPDH-F	GGAGCGAGATCCCTCCAAAAT	197
h-GAPDH-R	GGCTGTTGTCATACTTCTCATGG	
circRNA_006573-F	AAGATGAAAGGTCTGGCTGGC	137
circRNA_006573-R	GATGTCGCAAAGGCTTGCTTC	
circRNA_016395-F	CATCACCTTACTGCCCTCAGC	121
circRNA_016395-R	TGTGTTTCAGGACTGGGCAAAC	

## Wound Healing Assays

Transfected cells ( $2 \times 10^4$  per well) were harvested, plated in 6-well plates, and cultured until they reached 80% confluency. Subsequently, a 200  $\mu$ L pipette tip was used to draw a gap on the plates. After culture for 0 h, 24 h or 48 h, images were captured under an optical microscope (Z723975-1EA, Sigma, USA). Distance between the wound edges were quantified and compared with baseline values.

## Fluorescence in Situ Hybridization (FISH) Assays

FITC-labeled circ\_016395 and FITC-labeled circ\_006573 probes were designed and synthesized by GenePharma (Shanghai, China). A FISH kit (GenePharma, China) was used to measure probe signals. Transfected cells were fixed with 4% paraformaldehyde for 15 min and then washed with PBS 3 times for 5 min. Subsequently, the cells in each well were dehydrated overnight at 4°C in 70%, 85% and 100% ethanol and then hybridized with corresponding probes overnight in a dark and humid chamber at 37°C. After washing with SSC 3 times for 5 min, the cells were washed with PBS 3 times for 5 min at 37°C. They were then stained with DAPI for 10 min at 37°C and visualized on a fluorescence microscope (Ts2-FC, Nikon, Japan).

## Transwell Assays

Transfected cells were re-suspended ( $1 \times 10^4$  per well) in medium without FBS and plated (100  $\mu$ L) into upper chambers with inserts (3422, Costar, USA). The corresponding outside inserts were filled with complete medium (600  $\mu$ L). After 24 h, the cells in the upper compartment were removed using a cotton swab. Traversed cells on the lower side of the filter were fixed with 4% paraformaldehyde and stained with 0.1% crystal violet (C0121, Beyotime, China). Finally, images were captured using an optical microscope.

## Tube Formation Experiments

Transfected RAOEC cells ( $8 \times 10^2$  per well) were plated in 96-well plates that were precoated with Matrigel (354230, BD Biosciences, USA). After incubation at 37°C for 12 h, the tubular structures of transfected RAOEC cells were observed and captured under an optical microscope and quantified by ImageJ angiogenesis analyzer. The ImageJ software was used to assess the total length and number of segments, junctions, and meshes.

## Western Blot Assays

Transfected cells ( $1 \times 10^4$  per well) were lysed in RIPA buffer (P0013B, Beyotime, China) and centrifuged. The concentration of proteins was assessed using a BCA kit (P0010, Beyotime, China). After electrophoresis, the proteins were transferred onto PVDF membranes, blocked with 5% non-fat milk, and incubated with corresponding primary antibodies at 4°C overnight followed by secondary antibody for 1 h at 37°C. The immunoblots were developed with a color reagent (C500044, Sangon, China) and examined using an ECL Detection System (A44114, Invitrogen, USA). The band intensities were scanned using Image Lab software. Proteins were normalized to  $\beta$ -Actin. The anti-cebpb (1:1000, ab32358, 36 kDa), anti-IL-18 (1:1000, ab191860, 22 kDa), anti-VEGF-A (1:1000, ab214424, 27 kDa), anti- $\beta$ -Actin (1:20000, ab198991, 42 kDa), anti-Bcl-2 (1:1000, ab196495, 26 kDa), and anti-Bax (1:1000, ab32503, 21 kDa) primary antibodies were acquired from Abcam. The anti-Pscr1 (1:1000, abx114492, 35 kDa) primary antibodies were acquired from Abexa. The anti-Caspase-3 (1:1000, Asp175-5A1E, 17~19 kDa) primary antibodies were acquired from CST.

## Adeno-associated Virus Vector

Circ\_006573 shRNA recombinant AAV was constructed and synthesized by ShanDong ViGene Co., Ltd. (China). The infection efficiency of the circ\_006573 shRNA AAV was analyzed by fluorescence microscopy. Based on the viral titer ( $0.9 \times 10^9$  TU/mL), the AAV-circ\_006573 shRNA was diluted to  $0.5 \times 10^9$  TU/mL. An AVV vector expressing only green fluorescent protein (AAV-GFP) was also generated as the NC and used at the same titer.

## Animal Care

A total of 18 adult male Sprague-Dawley rats (SPF grade, weighing 200–250 g) were obtained from Shanghai SLAC Laboratory Animal Co., Ltd. (China). All animal protocols in our study were approved by the Animal Ethics Committee of Renji hospital. The animal protocols met the guidelines of the China Animal Care and Use Committee. The animals were housed in a clean facility under a controlled temperature of 22–24°C, relative humidity of 30–50%, and a 12-h day-night cycle.

## Establishment of a Rat SCI Model for Evaluating circ\_006573 Function

Rats were anesthetized with 2% pentobarbital sodium (30 mg/kg, ip) and placed on an operating table in a prone position [39]. After anesthesia, an incision was made along the

dorsal midline of the spine centered on the T10 vertebrae. Laminectomy was performed under an operating microscope to reveal ~3 mm dura of the spine. Then, the spinal cord was impacted according to a standardized modified Allen's method [40] using a controlled impact device (68097, RWD, China) with a drop hammer weight of 8 g and a drop height of 40 mm. Laminectomy was performed only in the Sham group.

After SCI, we used a microsyringe to inject 6  $\mu$ L AAV-circ\_006573 shRNA ( $3 \times 10^6$  TU) into the injured spinal cord of the SCI + AAV group. The SCI and Sham groups were injected with the same dose of empty AAV vector. After injection, the back tissue of each rat was sutured layer by layer, and then the rats were returned to clean cages.

## Motor Function Analysis

The Basso, Beattie, Bresnahan (BBB) Locomotor Rating Scale was used to estimate the recovery of ground locomotion [41]. The motor function of the hind limbs was recorded and scored by two individuals who were blinded to the experimental groups.

## Immunofluorescence Assays

On the 28th day after SCI, rats were anesthetized and perfused with 150 mL normal saline (ST341, Beyotime, China) through the heart, and the right atrial appendage was incised at the same time. After the effluent was clarified, the rats

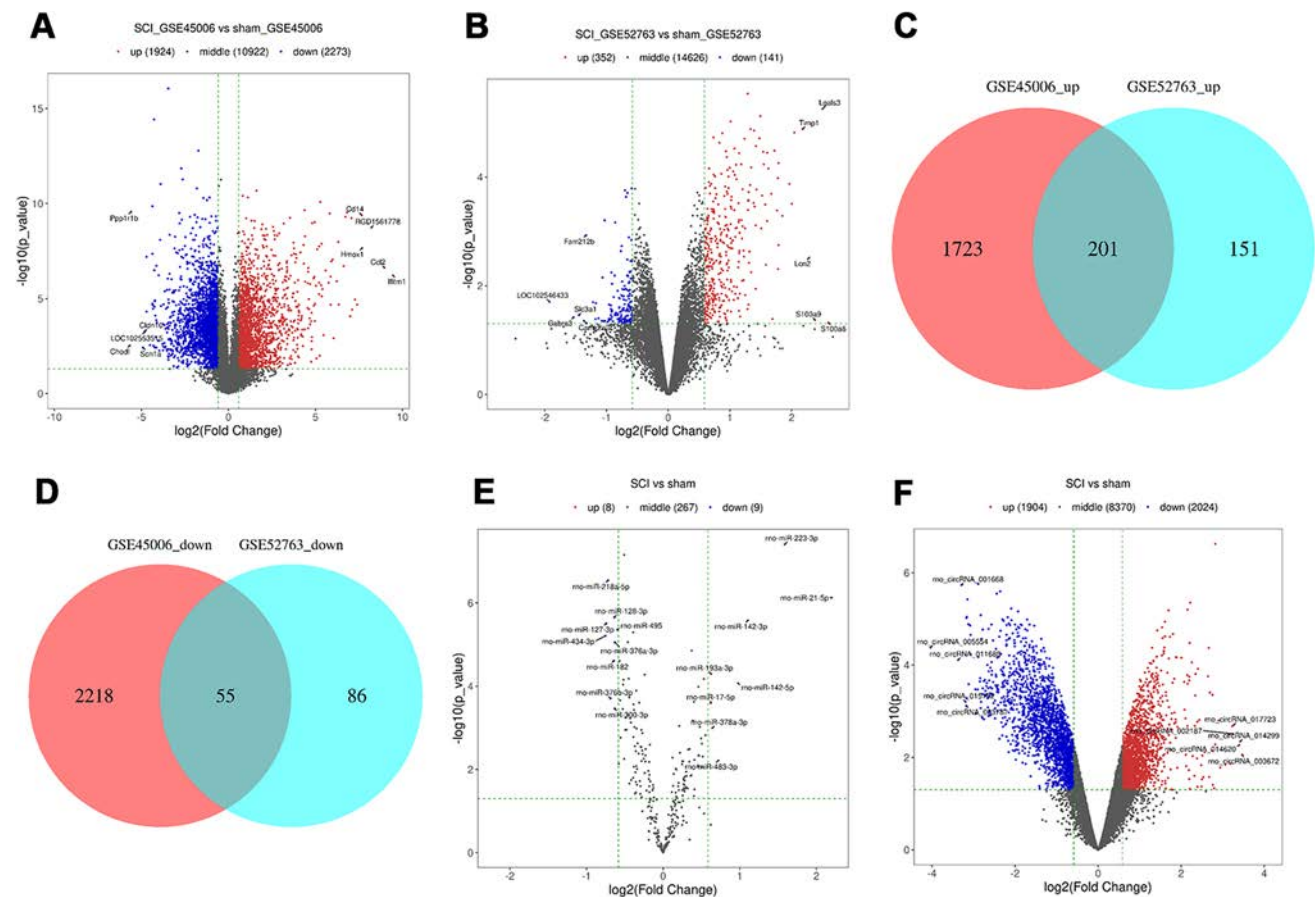


**Fig. 1** Differentially expressed RNAs in spinal cord injury (SCI). **A** Volcano map of differentially expressed mRNAs in the GSE45006 dataset. A total of 4197 mRNAs (1924 up-regulated and 2273 down-regulated) were obtained. **B** Volcano map of differentially expressed mRNAs in the GSE5276 dataset. A total of 493 mRNAs (352 up-regulated and 141 down-regulated) were obtained. **C** Venn diagram of up-regulated mRNAs in the two datasets. 201 up-regulated mRNAs were obtained after the intersection of the two sets of data. **D** Venn diagram of down-regulated mRNAs in the

two datasets. 55 down-regulated mRNAs were obtained. **E** Volcano map of differentially expressed miRNAs in the GSE19890 dataset. A total of 17 miRNAs (8 up-regulated and 9 down-regulated) were obtained. **F** Volcano map of differentially expressed circRNAs in the GSE114426 dataset. A total of 3928 circRNAs (1904 up-regulated and 2024 down-regulated) were obtained. Each dot represents an individual RNA molecule. Blue dots indicate down-regulated expression; Gray dots indicate no significant change in expression; and Red dots indicate up-regulated expression.

were perfused with 300 mL of 4% paraformaldehyde (P0099, Beyotime, China) until the tissues hardened. The spinal cord tissues around the injured site were removed and placed in 4% paraformaldehyde overnight. The tissues were then dehydrated and embedded in paraffin. Paraffin blocks were cut into 10  $\mu$ m slices with an Ultrathin microtome (Leica USA).

For immunofluorescence assays, the prepared slices were dewaxed and rehydrated. Antigen retrieval was carried out by boiling slices in 10 mM sodium citrate buffer (pH 9.0, 80°C) for 30 min. After sealing with 5% normal goat serum, the slices were incubated at 4°C overnight with diluted anti-CD31 antibody (AF6191, Affinity, USA), and subsequently

with secondary antibody (Alexa Fluor® 488, ab150077, Abcam, UK) at 37°C for 1 h. Images were captured using a fluorescence microscope.

## H&E Staining

After xylol dewaxing, slices were rehydrated with reducing concentrations of ethanol. They were then rinsed and stained with hematoxylin (G1004, Servicebio, China), 1% hydrochloric acid, and 1% eosin solution (C0109, Beyotime, China), followed by dehydration. After immersion in xylol and sealing in neutral gum, the tissue integrity was observed using an optical microscope.

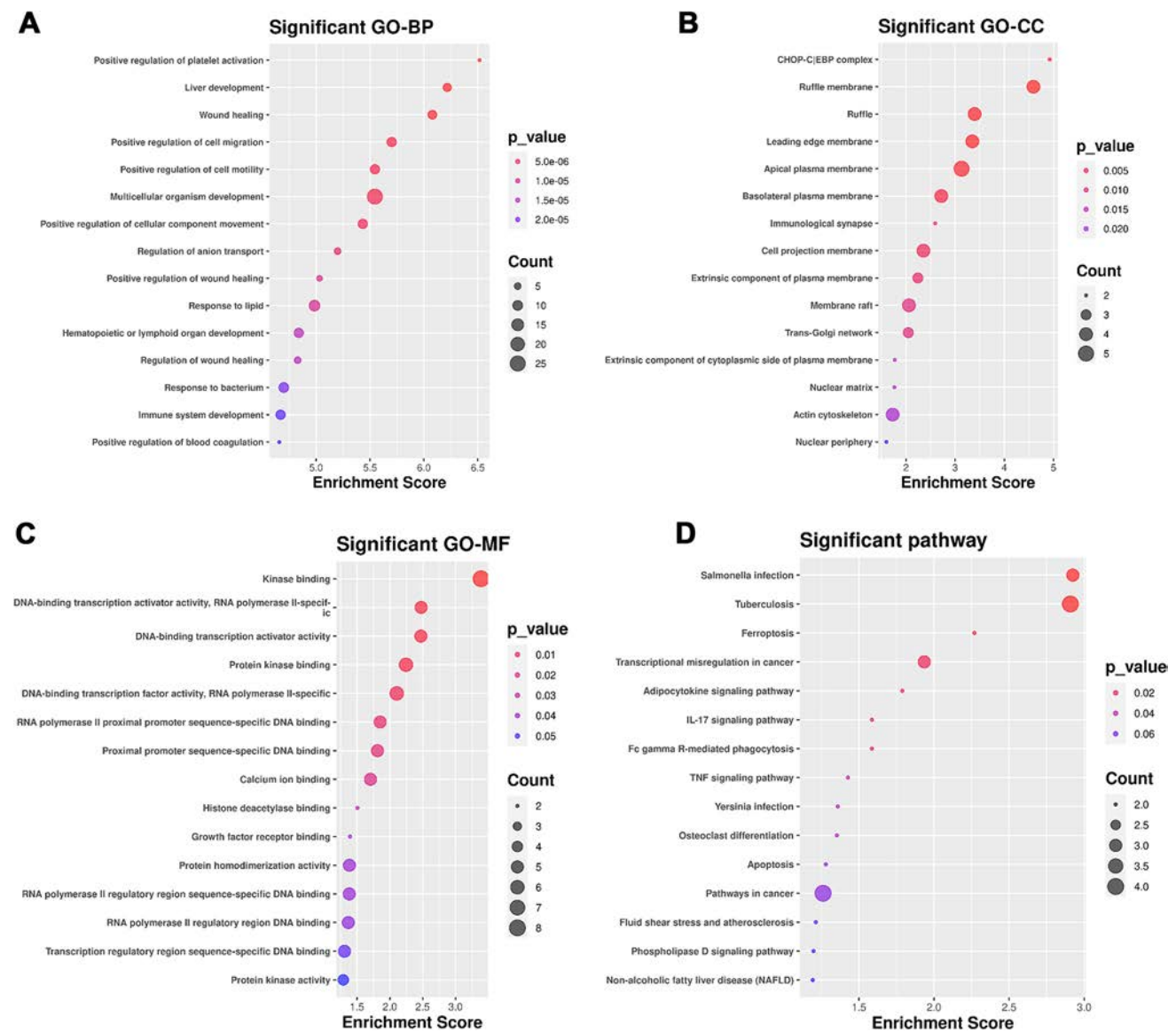


**Fig. 2.** Functional enrichment analysis of co-regulated genes in SCI. **A-C.** Bubble charts showing Gene Ontology pathways for differentially expressed RNAs that are co-regulated in GSE450063,

GSE5276, GSE19890, and GSE114426 datasets for GO-BPs (**A**), GO-CCs (**B**), and GO-MFs (**C**). **D** KEGG bubble chart. BP: biological process; CC: cellular component; MF: molecular function

### Immunohistochemistry (IHC) Assays

Slices were dewaxed, rehydrated, and rinsed with PBS. Then, the slices were subjected to antigen repair with 10 mM sodium citrate buffer (pH 9.0, 80°C, 30 min). After blocking,

the slices were treated with anti-CD34 antibody (1:2500, ab81289, Abcam, UK) or anti-CD31 antibody (1:2000, ab182981, Abcam, UK) overnight at 4°C, followed by reaction with secondary antibody (ab6721, Abcam, UK) at 37°C for 60 min. The slices were developed via DAB (abs9210,

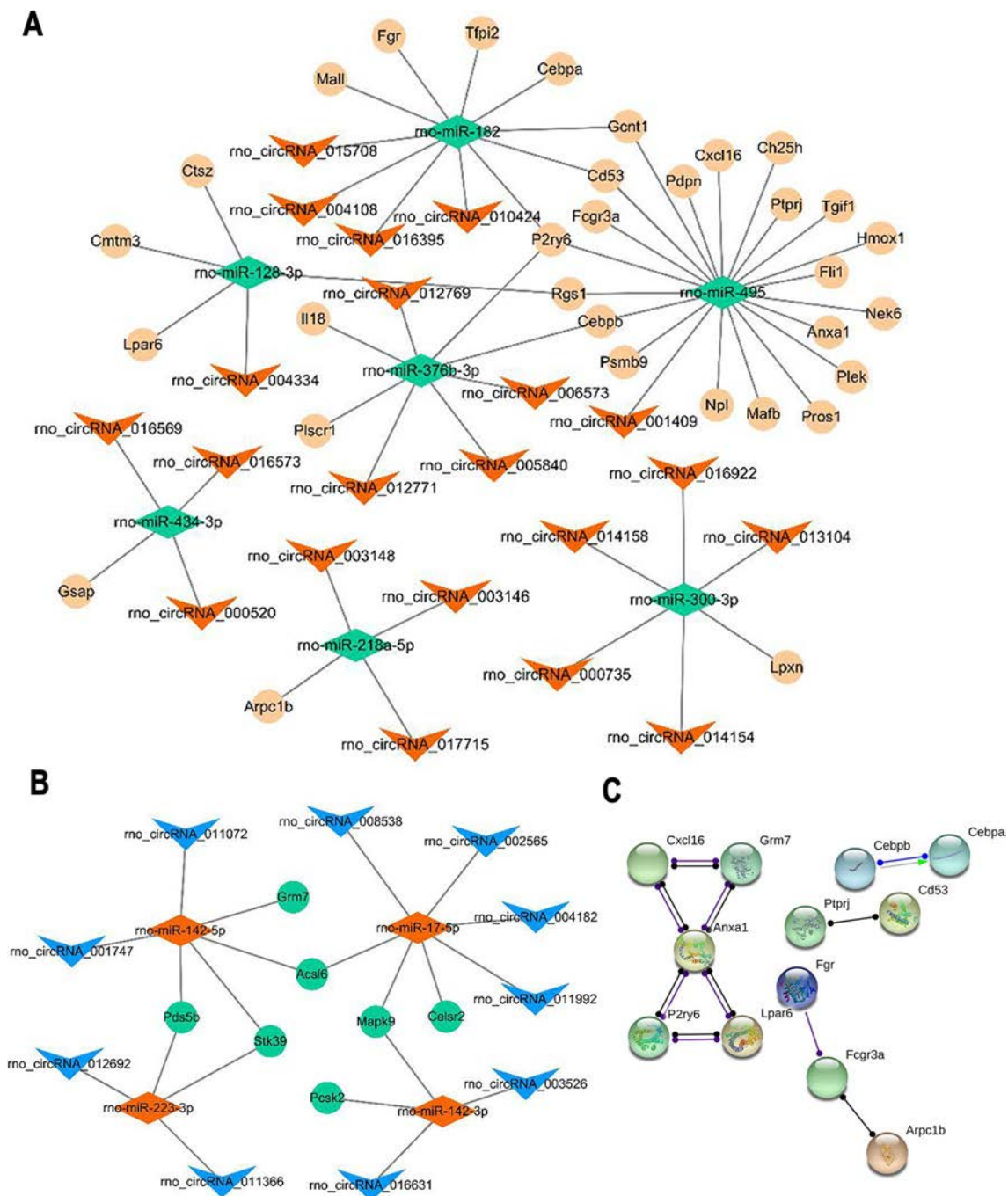


**Fig. 3** CircRNA-miRNA-mRNA network for SCI expression regulation. **A** Up\_circRNA-down\_miRNA-up\_mRNA network of coregulated RNAs in SCI. **B** Down\_circRNA-up\_miRNA-down\_mRNA network of coregulated RNAs in SCI. Diamond, V shape and circles

represent miRNAs, circRNAs, and mRNAs, respectively. **C** PPI network diagram of target genes in the SCI circRNA-miRNA-mRNA network.

Absin, China), dehydrated, and sealed with mounting medium. Images were observed and acquired under an optical microscope.

## Statistical Analysis

Data from at least three repeats were assessed utilizing GraphPad Prism 8.0 and are represented as the mean  $\pm$  standard deviation. Data comparisons were carried out utilizing one-way analysis of variance for multiple groups with the Tukey's post hoc test.  $P < 0.05$  was considered statistically meaningful.

## Results

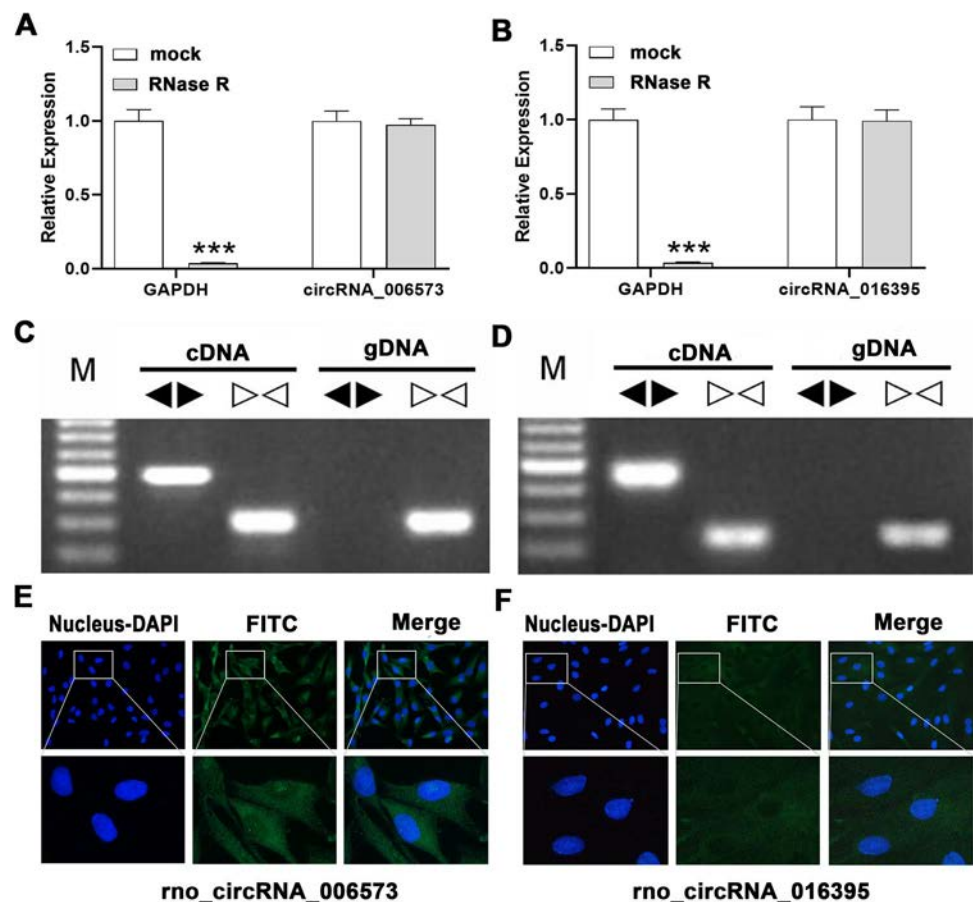
### Identification of a circRNA-miRNA-mRNA Network with Potential Function in Regulating SCI

To identify circRNA-miRNA-mRNA axes with potential function in SCI, we performed differential expression analysis of chip data from SCI and control rats in the Gene Expression Integration (GEO) database. A total of 4197 and 493 differentially expressed mRNAs were obtained from the

GSE45006 and GSE52763 datasets, respectively (Fig. 1A–1B). After the intersection of the two sets of data, 201 up-regulated mRNAs and 55 down-regulated mRNAs were obtained (Fig. 1C–1D). Additionally, seventeen differentially expressed miRNAs were obtained from the GSE19890 dataset (Fig. 1E), and 3928 differentially expressed circRNAs were obtained from the GSE114426 dataset (Fig. 1F). We used the databases(miRanda, miRDB, and miTarBase) to find the differential target genes corresponding to the differential miRNA, and obtain the relationship pair(up\_miRNA-down\_mRNA and down\_miRNA-up\_mRNA) existing in at least one database. Using the miRanda software package, we predicted the miRNA-circRNA binding relationship pair(up\_miRNA-down\_circRNA and down\_miRNA-up\_circRNA) according to the sequence of differential miRNA and differential circRNA. Finally, we screened 31 co-expressed circRNAs, 11 co-expressed miRNAs, and 39 co-expressed mRNAs to construct the circRNA-miRNA-mRNA network. The detailed lists are available in the supplementary data.

To evaluate the functions of the circRNA-miRNA-mRNA network, we performed Gene Ontology (GO) analysis. The top enrichment items were “positive regulation of platelet activation,” “liver development,” and “wound healing” in

**Fig. 4** Characterization of circ\_006573 and circ\_016395 circular structure and cytoplasmic localization. **A–B** Abundance of circ\_006573 and circ\_016395, as determined using quantitative real-time reverse transcriptase polymerase chain reaction (qRT-PCR), in RAOEC cells treated with or without RNase R. GAPDH served as a negative control. \*\*\*  $p < 0.001$ , compared with mock. **C–D** Convergent and divergent primers detect circ\_006573 and circ\_016395 in cDNA, but not in gDNA. cDNA, complementary DNA; gDNA, genomic DNA. **E–F** Fluorescence in situ hybridization (FISH) showing that circ\_006573 and circ\_016395 are mainly distributed in the cytoplasm of rat aortic endothelial cells (RAOECs) cells.



biological processes (BP) (Fig. 2A); “CHOP-C/EBP complex,” “ruffle membrane,” and “ruffle” in cellular components (CC) (Fig. 2B); and “kinase binding,” “DNA-binding transcription activator activity, RNA polymerase II-specific,” and “DNA-binding transcription activator activity” in molecular functions (MF) (Fig. 2C). Furthermore, in KEGG pathway enrichment analysis, the top three entries

were “salmonella infection,” “tuberculosis,” and “ferroptosis” (Fig. 2D).

To further evaluate how co-expressed RNAs within the circRNA-miRNA-mRNA axis may interact functionally, we performed network analysis using Cytoscape for visualization. The up\_circRNA-down\_miRNA-up\_mRNA network included 21 circRNA nodes, 7 miRNA nodes, 32 mRNA

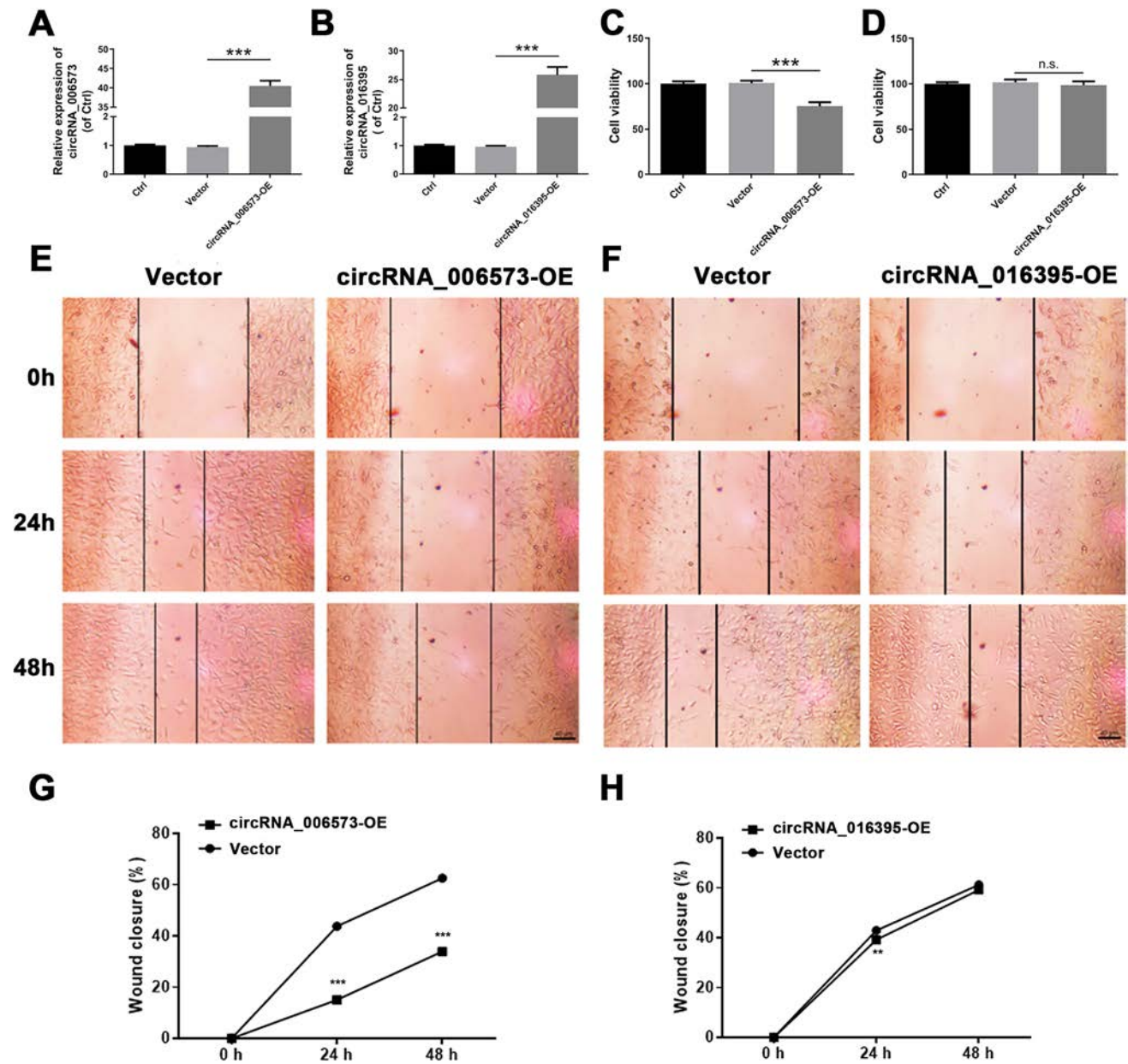


**Fig. 5** Circ\_006573, but not circ\_016395, suppresses the viability and migration of RAOEC cells. **A–B** The levels of circ\_006573 and circ\_016395 in RAOEC cells transfected with overexpression vectors were examined by qRT-PCR. \*\*\* $P < 0.001$ , compared with control. **C–D** The viability of RAOEC cells was examined by cell counting kit-8 assay at 24 h after transfection. Overexpressed circ\_006573 largely weakened the cell viability of RAOEC cells, whereas no sig-

nificant differences were observed for overexpressed circ\_016395. \*\*\* $P < 0.001$ ; n.s., not significant, compared with control. **E–H** The migration of RAOEC cells was examined by wound healing assays. Overexpression of circ\_006573, but not circ\_016395, blocked cell migration of RAOEC cells. \*\*\* $P < 0.001$ , \*\* $P < 0.01$ , compared with vector.

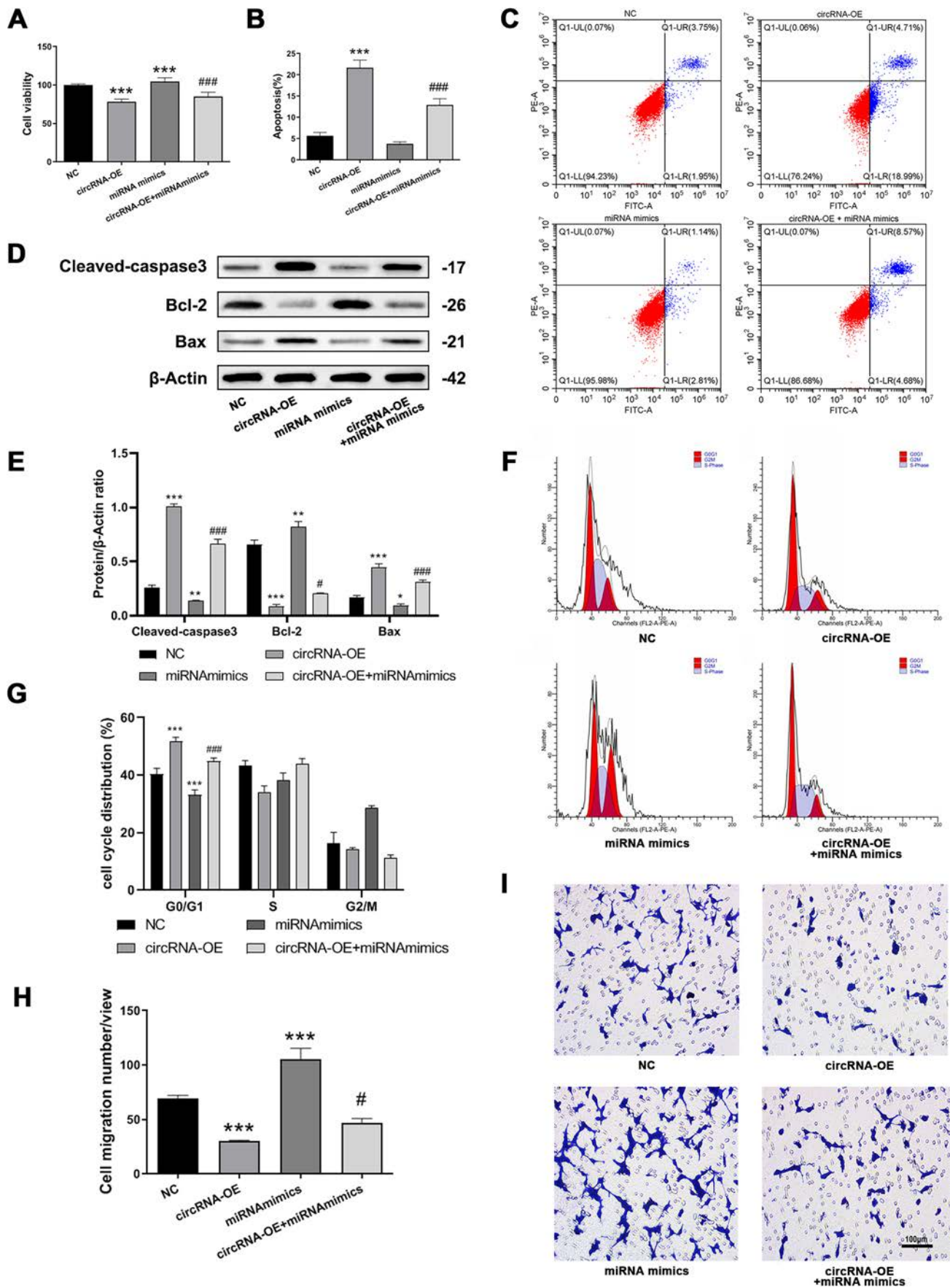


**Fig. 6** Effects of circ\_006573 up-regulation on the viability, apoptosis, cell cycle distribution and migration in RAOEC cells are rescued by MiR-376b-3p mimics. RAOEC cell viability was assessed by cell counting kit-8 assay (A) and apoptosis was assessed by flow cytometry (B, C) and Western blot (D, E) after transfection with circ\_006573 overexpression vector and/or MiR-376b-3p mimics. The miR-376b-3p mimics enhanced the cell viability and reversed the effect of circ\_006573 in suppressing cell viability (A). The circ\_006573 increased the apoptosis level in RAOEC cells, while overexpression miR-376b-3p mimics blocked RAOEC cell apoptosis and partially reversed the increased cell apoptosis after circ\_006573 overexpression (B-E).  $***P<0.001$ ,  $**P<0.01$ ,  $*P<0.05$ , compared with negative control (NC).  $###P<0.001$ ,  $#P<0.05$ , compared with circRNA-OE. Cell cycle distributions (F, G) were assessed by flow cytometry, and migration ability (H-I) was estimated by Transwell assay. The circ\_006573 overexpression induced cell cycle arrest in the G0/G1 phase, which was partially offset by miR-376b-3p mimics (F-G). Circ\_006573-mediated suppression of RAOEC cell migration was rescued by miR-376b-3p mimics, further suggesting that the biological functions of circ\_006573 may be mediated via regulation of miR-376b-3p (H-I).  $***P<0.001$ ,  $**P<0.01$ ,  $*P<0.05$ , compared with negative control (NC).  $###P<0.001$ ,  $#P<0.05$ , compared with circRNA-OE.

nodes, and 58 edges (Fig. 3A); and the down\_circRNA-up\_miRNA-down\_mRNA network included 10 circRNA nodes, 4 miRNA nodes, 7 mRNA nodes, and 21 edges (Fig. 3B). Next, we merged the mRNAs in the above two ceRNA networks and used the String online tool to construct a Protein-Protein Interaction (PPI) network, in which Anxa1 represented a key node and Cebpb and Cebpa were prominent (Fig. 3C). These results support potential important functions of the circRNA-miRNA-mRNA axis in regulating SCI via a network of proteins.

### Circ\_006573, but not circ\_016395, Affects Biological Behaviors in RAOEC Cells

To further explore the circRNA-miRNA-mRNA axis in SCI, we selected the top-ranked circ\_006573 and circ\_016395. First, we examined their stabilities and localization in RAOEC cells. Stability assays demonstrated that RNase R degraded almost all of the linear GAPDH mRNA, whereas circ\_006573 and circ\_016395 were strongly resistant to RNase R, confirming that these circRNAs harbor a loop structure (Fig. 4A-4B,  $P<0.001$ ). We also performed RT-PCR assays of circ\_006573 and circ\_016395 expression with convergent and divergent primers for cDNA or gDNA, which demonstrated that circ\_006573 and circ\_016395 only exist as cDNA (Fig. 4C-4D). These findings support the circular features of circ\_006573 and circ\_016395. Finally, we observed by FISH that circ\_006573 (Fig. 4E) and circ\_016395 (Fig. 4F) each were mainly distributed in the cytoplasm of RAOEC cells.

To analyze the biological functions of circ\_006573 and circ\_016395 on RAOEC cells, we transfected RAOEC cells with circ\_006573 and circ\_016395

overexpression plasmids (Fig. 5A-5B,  $P<0.001$ ). Overexpressed circ\_006573 largely weakened the cell viability of RAOEC cells as evaluated by CCK-8 assay (Fig. 5C,  $P<0.001$ ), whereas no significant differences were observed for overexpressed circ\_016395 (Fig. 5D,  $P>0.05$ ). Similarly, overexpression of circ\_006573, but not circ\_016395, blocked cell migration of RAOEC cells as evaluated by wound healing assay (Figs. 5E-H). Collectively, these results support a potential role for circ\_006573 in mediating the biological effects of SCI.

### Circ\_006573-induced Effects on Cell Viability, Migration, Angiogenesis, and Gene Expression in RAOEC Cells are Rescued by miR-376b-3p Mimics

To evaluate additional biological functions of circ\_006573, and to explore the potential role of a predicted target gene of circ\_006573, miR-376b-3p, we transfected circ\_006573 overexpressed plasmid, miR-376b-3p mimics and both into RAOEC cells, respectively. In CCK-8 assays, miR-376b-3p mimics enhanced the cell viability and reversed the effect of circ\_006573 in suppressing cell viability (Fig. 6A,  $P<0.001$ ). Moreover, the apoptosis levels detected by flow cytometry show that circ\_006573 increased the apoptosis level in RAOEC cells, while overexpression miR-376b-3p mimics blocked RAOEC cell apoptosis and partially reversed the increased cell apoptosis after circ\_006573 overexpression (Fig. 6B-C,  $P<0.001$ ). Western blot results of Caspase-3, Bcl-2 and Bax show that circ\_006573 overexpression led an increase of cell apoptosis (Fig. 6D-E,  $P<0.05$ ). Consistently, circ\_006573 overexpression induced cell cycle arrest in the G0/G1 phase, which was partially offset by miR-376b-3p mimics (Fig. 6F-G,  $P<0.05$ ). Furthermore, circ\_006573-mediated suppression of RAOEC cell migration was rescued by miR-376b-3p mimics, further suggesting that the biological functions of circ\_006573 may be mediated via regulation of miR-376b-3p. (Fig. 6H-I,  $P<0.05$ ).

Based on the GO pathways related to wound healing, we also considered the possibility that circ\_006573 may regulate angiogenesis during SCI. To clarify the role of circ\_006573/miR-376b-3p axis in regulating angiogenesis during SCI, circ\_006573 overexpression plasmid and miR-376b-3p mimics were separately and co-transfected into RAOEC cells. Tube formation assays demonstrated that overexpressed circ\_006573 repressed the total length, number of segments, junctions, and meshes in RAOEC cells, while miR-376b-3p mimics had the opposite effect (Fig. 7A-7E,  $P<0.05$ ). To evaluate potential downstream targets of circ\_006573, we also assessed its effects on the expression of Cebpb, IL-18, and Plscr1, each of which were predicted to be targeted by miR-376b-3p within the circRNA-miRNA-mRNA SCI network. Western blot and qRT-PCR

assays showed that circ\_006573 up-regulation decreased the Cebpb level and increased the IL-18 and Plscr1 level, while miR-376b-3p mimics had the opposite effect (Fig. 7F–7H,  $P < 0.05$ ). These results suggest that circ\_006573 targets miR-376b-3p to modulate cell viability, migration, angiogenesis, and gene regulation during SCI.

### Circ\_006573 shRNA Ameliorates Motor Function and Relieves the Pathological Morphology of the Spinal Cord Tissue in SCI Rats

To determine whether circ\_006573 may also have *in vivo* activity in modulating the pathology of SCI, we established a rat SCI model and prepared adeno-associated virus (AAV)-circ\_006573 shRNA and AAV-control shRNA, which we injected into injured spinal cords. Efficient transduction of the AAVs at equivalent levels for the circ\_006573 shRNA and control shRNA AAVs was verified by fluorescence in the spinal cords (Fig. 8A). The motor function of SCI rats was assessed according to the Basso, Beattie, Bresnahan (BBB) Locomotor Rating Scale. The results demonstrate that the BBB score was distinctly decreased in the SCI group (AAV-control shRNA + SCI) relative to the sham group (AAV-control shRNA only), while circ\_006573 shRNA (AAV\_006573 shRNA + SCI) enhanced the BBB score of SCI rats after a 28 day time course (Fig. 8B,  $P < 0.001$ ). To further visualize the pathophysiology, we performed H&E staining. In the sham group, the gray matter in the spinal cord was clearly demarcated, and the cell morphology was normal (Fig. 8C, first column), while in the SCI + AAV-control shRNA group, hemorrhages were seen in the gray matter of the spinal cord, and the ventral and ventrolateral white matter structure was notably loosened and vacuolized (Fig. 8C, middle column). In comparison, in the SCI + AAV-circ\_006573 shRNA group, the pathological injury of the spinal cord tissue was much less visible (Fig. 8C, third column). These results suggest that circ\_006573 shRNA may have therapeutic activity in the SCI rat model.

### Circ\_006573 shRNA Elevates the Expression of CD31, CD34, and VEGF-A in Spinal Cord Tissue in SCI Rats

CD34 and CD31 are commonly utilized as vascular endothelial markers [42]. Thus, we examined CD31 and CD34 expression in the SCI rat model by immunohistochemistry assay. Circ\_006573 shRNA treatment increased the expression of CD31 and CD34 in the spinal cord tissue of SCI rats (Fig. 9A, first and middle row). These findings were verified by immunofluorescence assay (Fig. 9A, third row), thus further validating the increase of angiogenesis in circ\_006573 shRNA-treated SCI lesions. As additional confirmation, Western blot assay revealed lower VEGF-A expression in the SCI-shRNA control group than in the sham group, while

the addition of circ\_006573 shRNA markedly increased the VEGF-A expression of the spinal cord tissue (Fig. 9B–9C,  $P < 0.001$ ). These results are consistent with an *in vivo* role of circ\_006573 in angiogenesis as a mechanism for ameliorating SCI outcomes.

## Discussion

With the development of microarray technology, RNA-seq and bioinformatics analysis, the dysregulation of ncRNA has been shown to correlate with pathological manifestations of SCI. For example, Chen et al. identified 16013 circRNAs and 960 miRNAs that were differentially expressed in SCI mice using RNA-seq technology, and among them, circPrkcs was increased dramatically in both *in vivo* and *in vitro* SCI models [43]. Moreover, Wang et al. identified 498 circRNAs, 458 lncRNAs, 155 miRNAs, and 1203 mRNAs that were differentially expressed in the TSCI mouse model using RNA-seq technology [44]. These reports suggest that the dysregulation of ncRNA can serve as a potential biomarker of SCI, thus supporting the benefit of characterizing roles for circRNAs in SCI. In this project, we used bioinformatics analysis to screen for differentially expressed mRNAs, miRNAs, and circRNAs in SCI rats and identified 4690 mRNAs, 17 miRNAs and 3928 circRNAs that were differentially expressed. We screened for co-expressed RNAs and finally chose the top-ranked circ\_006573 and circ\_016395 for further analysis.

CircRNAs exist as closed-loop structures in cells because the 5' and 3' ends are connected by covalent bonds [45]. Compared with linear RNAs, circRNAs have higher stability and conservatism due to their special structure [46]. In our study, we demonstrated that RNase R degraded the linear GAPDH mRNA almost to completion, while circ\_006573 and circ\_016395 were strongly resistant to RNase R, thus verifying that circ\_006573 and circ\_016395 harbor a loop structure. Cell sublocalization is critical to the biological function of ncRNA, and circRNAs have been found in viruses, archaea, and eukaryotes, most of which are localized to the cytoplasm [47]. We observed by FISH that circ\_006573 and circ\_016395 were mainly distributed in the cytoplasm of RAOEC cells, which is consistent with a potentially important cellular function of these circRNAs.

Numerous studies have identified circRNAs that are associated with SCI. For example, Li et al demonstrated that HIF-1 $\alpha$  suppresses inflammation in SCI via the miR-380-3p/NLRP3 axis and is regulated by circ\_0001723 [48]. Moreover, circ\_2960 facilitates secondary injury of SCI by targeting miRNA-124 [49]. Additionally, circ\_Plek facilitates fibrosis by modulating the miR-135b-5p/TGF- $\beta$ R1 axis after SCI [50]. Chen JN et al also demonstrated that circ\_Prkcs is overexpressed in SCI, and that silencing of

circ\_PrkcsH represses Ccl2 expression by enhancing miR-488 and weakens the inflammation in SCI [43]. Since these findings, circRNAs may have important functions in SCI. In this study, we added to previous understanding of the role of circRNAs in SCI by demonstrating that circ\_006573 overexpression largely weakens the viability and migration in

RAOEC cells. We also evaluated the effect of circ\_016395 overexpression but observed no obvious effects. Therefore, we chose circ\_006573 for subsequent experiments.

Bioinformatics analysis predicted that miR-376b-3p may have an interactive relationship with circ\_006573 in SCI, which we verified by functional analyses. MiR-376b-3p is

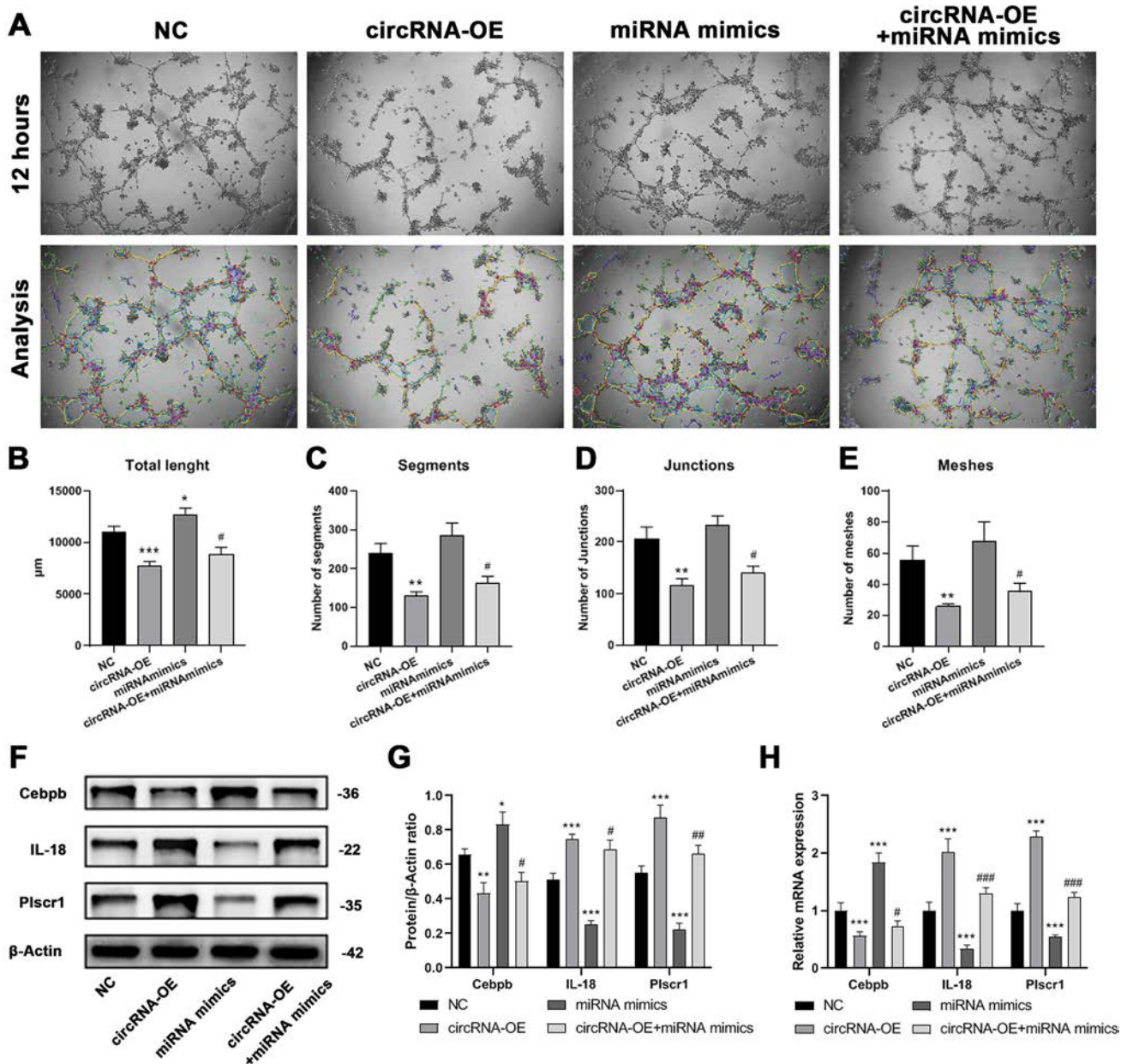


**Fig. 7** Circ\_006573 suppresses angiogenesis and modulates gene expression in RAOEC cells, which is rescued by MiR-376b-3p mimics. **A-E** The angiogenesis activity of RAOEC cells was measured by tube formation assay after transfection with circ\_006573 overexpression vector and/or MiR-376b-3p mimics. Using ImageJ software to quantify the tube formation (**A**), assess the total length (**B**) and number of segments (**C**), junctions (**D**), and meshes (**E**). Overexpressed circ\_006573 repressed the total length, number of segments, junctions, and meshes in RAOEC cells, while miR-376b-3p

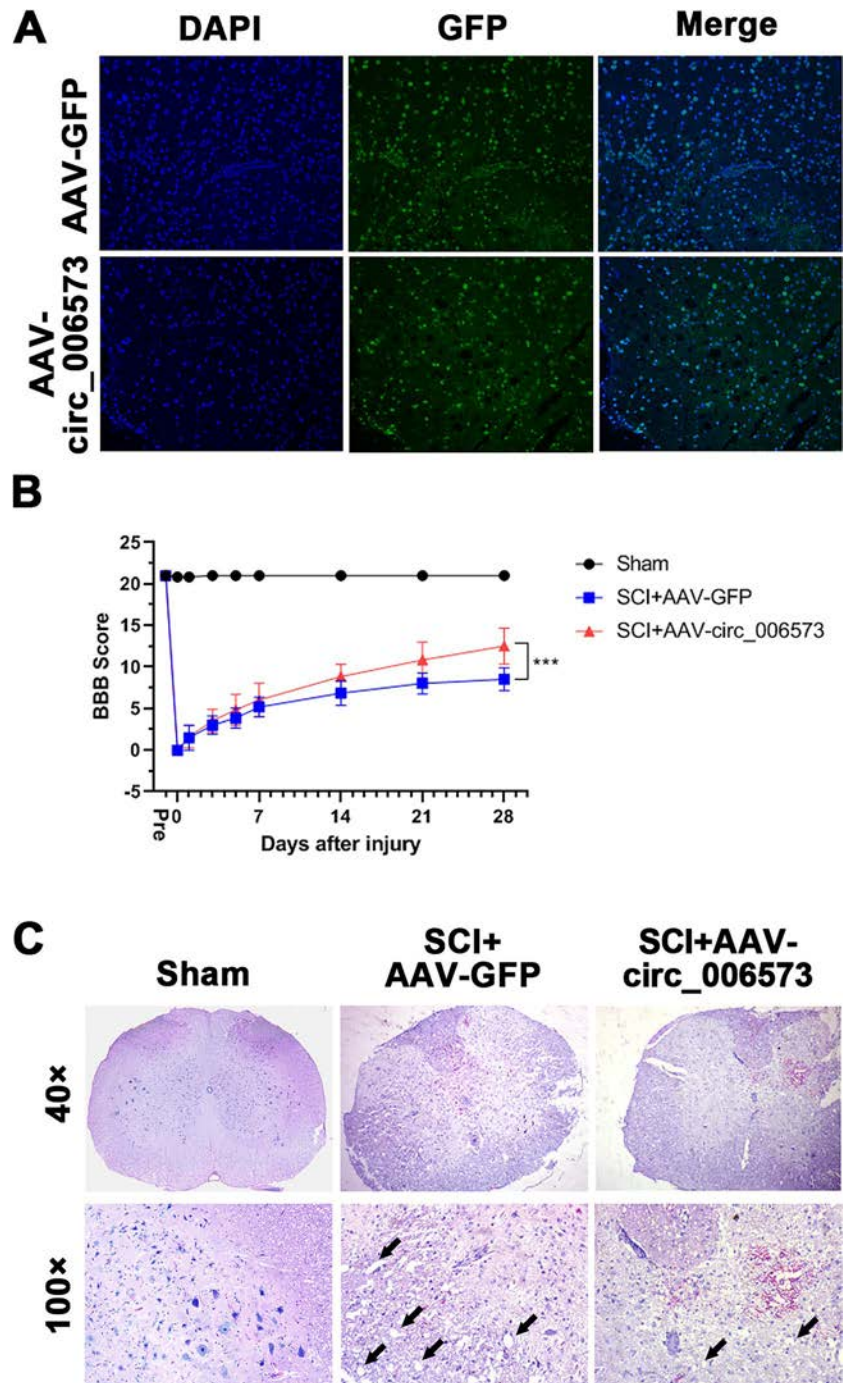
mimics had the opposite effect.  $***P < 0.001$ ,  $**P < 0.01$ ,  $*P < 0.05$ , compared with negative control (NC).  $#P < 0.05$ , compared with circRNA-OE. **F-H** Cebpb, IL-18, and Plscr1 levels in RAOEC cells were assessed by Western blot assay and qRT-PCR. The circ\_006573 up-regulation decreased the Cebpb level and increased the IL-18 and Plscr1 level (**F-H**), while miR-376b-3p mimics had the opposite effect (**H**)  $*P < 0.05$ ,  $**P < 0.01$ ,  $***P < 0.001$  vs. negative control (NC).  $###P < 0.001$ ,  $##P < 0.01$ ,  $#P < 0.05$ , compared with circRNA-OE.

known to participate in the development of diverse human diseases, including tumor progression, angiogenesis, and liver regeneration [51, 52]. Evidence suggests that miR-376b-3p promotes the malignant progression of NSCLC by targeting KLF15 [53]. In this study, we also determined that miR-376b-3p has low expression in SCI. MiR-376b-3p mimic increased the viability, migration, and angiogenesis of RAOEC cells, and decreased the apoptosis. Importantly, miR-376b-3p mimic reversed the function of circ\_006573 overexpression on the latter biological behaviors, suggesting

that it may promote healing during SCI by reversing the effects of circ\_006573.

The circRNA-miRNA-mRNA network identified in this study predicted that miR-376b-3p, which interacts with circ\_006573, directly regulates Cebpb, IL-18, and Plscr1. Western blot assays verified that circ\_006573 up-regulation reduced Cebpb levels and increased the expression of IL-18 and Plscr1, while miR-376b-3p mimics reversed this effect. These results are consistent with the PPI network identified in our bioinformatics analysis, which included Cebpb [54],

**Fig. 8** Circ\_006573 shRNA ameliorates motor function and relieves the pathological appearance of the spinal cord tissue in SCI rats. **A** The infection efficiency of adeno-associated virus (AAV) after injection was examined under a fluorescence microscope. **B** BBB scores in the Sham, SCI+AAV-GFP, and SCI+AAV-circ\_006573 groups at 28 days after injection, demonstrate that circ\_006573 shRNA (SCI+AAV-circ\_006573) enhanced the BBB score of SCI rats after a 28 day time course. \*\*\* $P < 0.001$ , compared with SCI+AAV-GFP. **C** H&E staining of spinal cord tissue in the above 3 groups of SCI rats. The black arrows show the vacuolized changes in the spinal cord tissue. The cell morphology was normal (first column), while in the SCI + AAV-control shRNA group, hemorrhages were seen in the gray matter of the spinal cord, and the ventral and ventrolateral white matter structure was notably loosened and vacuolized (middle column). In comparison, in the SCI + AAV-circ\_006573 shRNA group, the pathological injury of the spinal cord tissue was much less visible (third column). These results suggest that circ\_006573 shRNA may have therapeutic activity in the SCI rat model.



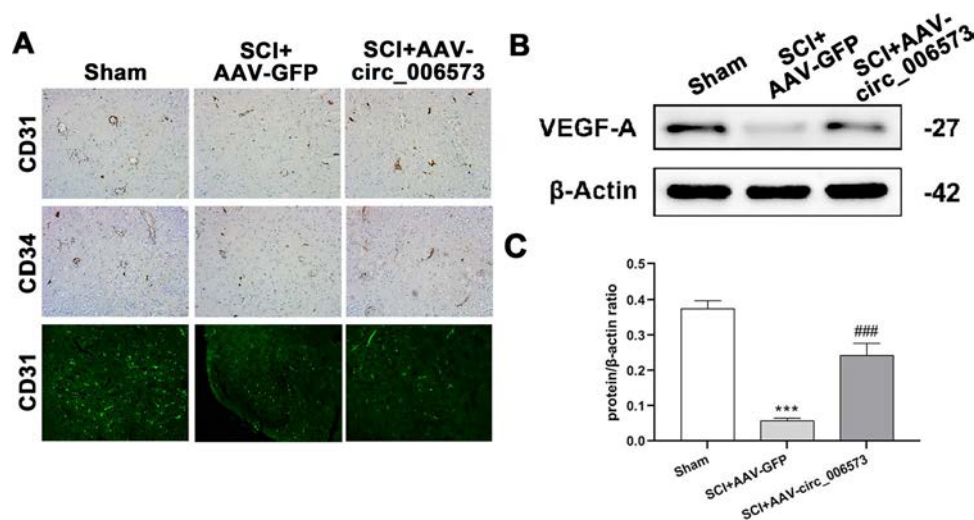


**Fig. 9** Circ\_006573 shRNA increases the expression of CD31, CD34 and VEGF-A in spinal cord tissue after SCI. **A** CD31 and CD34 expression was examined by immunohistochemistry assay 28 days after sham treatment, SCI and injection of SCI+AAV-GFP, and SCI+AAV-circ\_006573. The expression of CD31 in spinal cord tissue was examined by immunofluorescence. Circ\_006573 shRNA treatment increased the expression of CD31 and CD34 in the spinal cord tissue of SCI rats (first and middle row). These findings were verified by immunofluorescence assay (third row), thus further vali-

dating the increase of angiogenesis in circ\_006573 shRNA-treated SCI lesions. **B-C** The expression of VEGF-A in spinal cord tissue was examined by Western blot, revealed lower VEGF-A expression in the SCI-shRNA control group than in the sham group, while the addition of circ\_006573 shRNA markedly increased the VEGF-A expression of the spinal cord tissue. These results are consistent with an *in vivo* role of circ\_006573 in angiogenesis as a mechanism for ameliorating SCI outcomes. \*\*\* $P < 0.001$ , compared with Sham. ### $P < 0.001$ , compared with SCI+AAV-GFP.

a regulator of inflammation. Thus, these findings support the circRNA-miRNA-mRNA network as a tool for regulating the pathological effects of SCI.

To evaluate the *in vivo* relevance of our findings, we employed a rat SCI model that has been established to recapitulate the pathological mechanisms of SCI and is useful for measuring the effectiveness of experimental treatment measures [55]. To assess circ\_006573 function, we injected AAV-circ\_006573 shRNA into injured spinal cords. According to the Basso, Beattie, Bresnahan (BBB) Locomotor Rating Scale, which estimates the recovery of ground locomotion [41], the SCI group at 28 days had a low BBB score relative to the sham group, while circ\_006573 shRNA enhanced the BBB score in SCI rats. We further examined the effect of AAV-circ\_006573 shRNA on the pathology of SCI by H&E staining, which has previously been used to assess the SCI severity [56]. In the SCI group, hemorrhages were seen in the gray matter of the spinal cord, and the ventral and ventrolateral white matter structures were notably loosened and vacuolized. Notably, circ\_006573 shRNA reduced the pathological injury of the spinal cord tissue in SCI rats, suggesting the therapeutic potential of targeting circ\_006573.

Angiogenesis is pivotal for the repair of SCI. Damage caused by local vascular loss and blood-brain barrier injury can lead to ischemia and inflammation, leading to comprehensive injury of spinal cord nerve tissue [57].

Furthermore, CD34 and CD31 are commonly utilized as vascular endothelial markers that reflect the status of microvessels and are therefore critical factors for quantitative evaluation of angiogenesis [42, 58]. After SCI, cyclic citrullinated peptide (CCP) intervention for 7 and 14 days has been shown to enhance angiogenesis by increasing the mRNA levels of CD31 in the spinal cord tissue [59]. We demonstrated that circ\_006573 shRNA treatment increased the expression of CD31 and CD34 in spinal cord tissues of SCI rats. Moreover, VEGF-A expression was lower in the SCI group than in the sham group, and circ\_006573 shRNA markedly augmented its expression. Thus, these results provide additional support for an important role of circ\_006573 in suppressing angiogenesis during SCI.

In conclusion, by utilizing a comprehensive strategy involving big data mining and computational biology, we constructed a circRNA-miRNA-mRNA network and demonstrated that circ\_006573 may serve a key role as a ceRNA in SCI. The circRNA-miRNA-mRNA axis identified in this study could offer a foundation for comprehending pathophysiological mechanisms of SCI, as well as for informing the development of new cure strategies.

**Availability of Data and Material** All data generated or analysed during this study are included in this published article [and its supplementary information files].

**Supplementary Information** The online version contains supplementary material available at <https://doi.org/10.1007/s12035-023-03357-0>.

**Acknowledgements** Not applicable.

**Authors' Contributions** These authors contributed equally to this work: K. Wang, Q-X. Song, and X-J. Su. K. Wang, C. Zhu, and H-X. Shen designed the experiments and wrote the manuscript. K. Wang, Q-X. Song, and X-J. Su performed the experiments. Z. Chen, H. Chen, and Y-C. Han carried out the data analyses. C. Zhu, and H-X. Shen contributed to the editing, revision, and final approval of the manuscript. All authors read and approved the final manuscript.

**Funding** The research was supported by Natural Science Foundation of China (81802139, 81870885), Shanghai Outstanding academic leaders plan of Shanghai Municipal Science and Technology Committee (18XD1402300), Medical-Engineering Joint Fund of Shanghai Jiao Tong University (YG2017QN51), and Cultivating Fund of Renji Hospital (PYII-17-011).

## Declarations

**Ethics Approval and Consent to Participate** All animal protocols in our study were approved by the Animal Ethics Committee of Renji hospital. The animal protocols met the guidelines of the China Animal Care and Use Committee.

**Consent for Publication** Not applicable.

**Competing Interests** The authors declare that they have no competing interests.

## References

- Jiang JP, Liu XY, Zhao F, Zhu X, Li XY, Niu XG, Yao ZT, Dai C et al (2020) Three-dimensional bioprinting collagen/silk fibroin scaffold combined with neural stem cells promotes nerve regeneration after spinal cord injury. *Neural Regen Res* 15:959–968
- Holmes D (2017) Spinal-cord injury: spurring regrowth. *Nature* 552:S49
- Hu XC, Lu YB, Yang YN, Kang XW, Wang YG, Ma B, Xing S (2021) Progress in clinical trials of cell transplantation for the treatment of spinal cord injury: how many questions remain unanswered? *Neural Regen Res* 16:405–413
- Schreiber AF, Garlasco J, Vieira F, Lau YH, Stavi D, Lightfoot D, Rigamonti A, Burns K et al (2021) Separation from mechanical ventilation and survival after spinal cord injury: a systematic review and meta-analysis. *Ann Intensive Care* 11:149
- Anjum A, Yazid MD, Fauzi Daud M, Idris J, Ng AMH, Selvi Naicker A, Ismail OH, Athi Kumar RK et al (2020) Spinal Cord Injury: Pathophysiology, Multimolecular Interactions, and Underlying Recovery Mechanisms. *Int J Mol Sci* 21(20):7533
- Ahuja CS, Wilson JR, Nori S, Kotter MRN, Druschel C, Curt A, Fehlings MG (2017) Traumatic spinal cord injury. *Nat Rev Dis Primers* 3:17018
- Donovan J, Kirshblum S (2018) Clinical Trials in Traumatic Spinal Cord Injury. *Neurotherapeutics* 15:654–668
- Uldreaj A, Chio JC, Ahuja CS, Fehlings MG (2016) Modulating the immune response in spinal cord injury. *Expert Rev Neurother* 16:1127–1129
- Hara M, Kobayakawa K, Ohkawa Y, Kumamaru H, Yokota K, Saito T, Kijima K, Yoshizaki S et al (2017) Interaction of reactive astrocytes with type I collagen induces astrocytic scar formation through the integrin-N-cadherin pathway after spinal cord injury. *Nat Med* 23:818–828
- Wang W, Su Y, Tang S, Li H, Xie W, Chen J et al (2019) Identification of noncoding RNA expression profiles and regulatory interaction networks following traumatic spinal cord injury by sequence analysis. *Aging* 11:2352–2368
- Gao L, Peng Y, Xu W, He P, Li T, Lu X, Chen G (2020) Progress in Stem Cell Therapy for Spinal Cord Injury. *Stem Cells Int* 2020:2853650
- Figley SA, Khosravi R, Legasto JM, Tseng YF, Fehlings MG (2014) Characterization of vascular disruption and blood-spinal cord barrier permeability following traumatic spinal cord injury. *J Neurotrauma* 31:541–552
- Ni S, Luo Z, Jiang L, Guo Z, Li P, Xu X, Cao Y, Duan C et al (2019) UTX/KDM6A Deletion Promotes Recovery of Spinal Cord Injury by Epigenetically Regulating Vascular Regeneration. *Mol Ther* 27:2134–2146
- Cao Y, Xu Y, Chen C, Xie H, Lu H, Hu J (2021) Local delivery of USC-derived exosomes harboring ANGPTL3 enhances spinal cord functional recovery after injury by promoting angiogenesis. *Stem Cell Res Ther* 12:20
- Gris D, Marsh DR, Oatway MA, Chen Y, Hamilton EF, Dekaban GA, Weaver LC (2004) Transient blockade of the CD11d/CD18 integrin reduces secondary damage after spinal cord injury, improving sensory, autonomic, and motor function. *J Neurosci* 24:4043–4051
- Han S, Arnold SA, Sithu SD, Mahoney ET, Geraldts JT, Tran P, Benton RL, Maddie MA et al (2010) Rescuing vasculature with intravenous angiopoietin-1 and alpha v beta 3 integrin peptide is protective after spinal cord injury. *Brain J Neurol* 133:1026–1042
- Rust R, Grönnert L, Gantner C, Enzler A, Mulders G, Weber RZ, Siewert A, Limasale YD et al (2019) Nogo-A targeted therapy promotes vascular repair and functional recovery following stroke. *Proc Natl Acad Sci U S A* 116:14270–14279
- Zörner B, Schwab ME (2010) Anti-Nogo on the go: from animal models to a clinical trial. *Ann N Y Acad Sci* 1198(Suppl 1):E22–E34
- Kleaveland B, Shi CY, Stefano J, Bartel DP (2018) A Network of Noncoding Regulatory RNAs Acts in the Mammalian Brain. *Cell* 174:350–62.e17
- Ning B, Gao L, Liu RH, Liu Y, Zhang NS, Chen ZY (2014) microRNAs in spinal cord injury: potential roles and therapeutic implications. *Int J Biol Sci* 10:997–1006
- Sun F, Li SG, Zhang HW, Hua FW, Sun GZ, Huang Z (2020) miRNA-411 attenuates inflammatory damage and apoptosis following spinal cord injury. *Eur Rev Med Pharmacol Sci* 24:491–498
- Bai G, Jiang L, Meng P, Li J, Han C, Wang Y, Wang Q (2021) LncRNA Neat1 Promotes Regeneration after Spinal Cord Injury by Targeting miR-29b. *J Mol Neurosci* 61:1174–1184
- Yao Y, Wang J, He T, Li H, Hu J, Zheng M, Ding Y, Chen YY et al (2020) Microarray assay of circular RNAs reveals circRNA.7079 as a new anti-apoptotic molecule in spinal cord injury in mice. *Brain Res Bull* 164:157–171
- Chen LL, Yang L (2015) Regulation of circRNA biogenesis. *RNA Biol* 12:381–388
- Yao C, Yu B (2019) Role of Long Noncoding RNAs and Circular RNAs in Nerve Regeneration. *Front Mol Neurosci* 12:165
- Zhou ZB, Niu YL, Huang GX, Lu JJ, Chen A, Zhu L (2018) Silencing of circRNA.2837 Plays a Protective Role in Sciatic Nerve Injury by Sponging the miR-34 Family via Regulating Neuronal Autophagy. *Molecular therapy Nucleic acids* 12:718–729
- Zhou ZB, Du D, Chen KZ, Deng LF, Niu YL, Zhu L (2019) Differential Expression Profiles and Functional Predication of

- Circular Ribonucleic Acid in Traumatic Spinal Cord Injury of Rats. *J Neurotrauma* 36:2287–2297
28. Qin C, Liu CB, Yang DG, Gao F, Zhang X, Zhang C, Du LJ YML et al (2018) Circular RNA Expression Alteration and Bioinformatics Analysis in Rats After Traumatic Spinal Cord Injury. *Front Mol Neurosci* 11:497
  29. Zhou R, Wu Y, Wang W, Su W, Liu Y, Wang Y, Fan C, Li X et al (2018) Circular RNAs (circRNAs) in cancer. *Cancer Lett* 425:134–142
  30. Chu KJ, Ma YS, Jiang XH, Wu TM, Wu ZJ, Li ZZ, Wang JH, Gao QX et al (2020) Whole-Transcriptome Sequencing Identifies Key Differentially Expressed mRNAs, miRNAs, lncRNAs, and circRNAs Associated with CHOL. *Mol Ther Nucleic Acids* 21:592–603
  31. Lu Q, Liu T, Feng H, Yang R, Zhao X, Chen W, Jiang B, Qin H et al (2019) Circular RNA circSLC8A1 acts as a sponge of miR-130b/miR-494 in suppressing bladder cancer progression via regulating PTEN. *Mol Cancer* 18:111
  32. Feng J, He W, Xia J, Huang Q, Yang J, Gu WP, Zhang N, Liu YH (2023) Human umbilical cord mesenchymal stem cells-derived exosomal circDLGAP4 promotes angiogenesis after cerebral ischemia-reperfusion injury by regulating miR-320/KLF5 axis. *FASEB J* 37:e22733
  33. Huang X, Chen Y, Xiao J, Huang Z, He L, Xu D, Peng J (2018) Identification of differentially expressed circular RNAs during TGF- $\beta$ 1-induced endothelial-to-mesenchymal transition in rat coronary artery endothelial cells. *Anatol J Cardiol* 19:192–197
  34. Liu W, Jia C, Luo L, Wang HL, Min XL, Xu JH, Ma LQ, Yang XM et al (2019) Novel circular RNAs expressed in brain microvascular endothelial cells after oxygen-glucose deprivation/recovery. *Neural Regen Res* 14:2104–2111
  35. Barrett T, Wilhite SE, Ledoux P, Evangelista C, Kim IF, Tomashevsky M, Marshall KA, Phillippy KH et al (2013) NCBI GEO: archive for functional genomics data sets--update. *Nucleic Acids Res* 41:D991–D995
  36. Ritchie ME, Phipson B, Wu D, Hu Y, Law CW, Shi W, Smyth GK (2015) limma powers differential expression analyses for RNA-seq and microarray studies. *Nucleic Acids Res* 43:e47
  37. Shannon P, Markiel A, Ozier O, Baliga NS, Wang JT, Ramage D, Amin N, Schwikowski B et al (2003) Cytoscape: a software environment for integrated models of biomolecular interaction networks. *Genome Res* 13:2498–2504
  38. Szklarczyk D, Franceschini A, Wyder S, Forslund K, Heller D, Huerta-Cepas J, Simonovic M, Roth A et al (2015) STRING v10: protein-protein interaction networks, integrated over the tree of life. *Nucleic Acids Res* 43:D447–D452
  39. Zhong ZX, Feng SS, Chen SZ, Chen ZM, Chen XW (2019) Inhibition of MSK1 Promotes Inflammation and Apoptosis and Inhibits Functional Recovery After Spinal Cord Injury. *J Mol Neurosci* 68:191–203
  40. Hu J, Yang Z, Li X, Lu H (2016) C-C motif chemokine ligand 20 regulates neuroinflammation following spinal cord injury via Th17 cell recruitment. *J Neuroinflammation* 13:162
  41. Basso DM, Beattie MS, Bresnahan JC (1995) A sensitive and reliable locomotor rating scale for open field testing in rats. *J Neurotrauma* 12:1–21
  42. Wu Y, Li Z, Xiu AY, Meng DX, Wang SN, Zhang CQ (2019) Carvedilol attenuates carbon tetrachloride-induced liver fibrosis and hepatic sinusoidal capillarization in mice. *Drug Des Devel Ther* 13:2667–2676
  43. Chen JN, Zhang YN, Tian LG, Zhang Y, Li XY, Ning B (2022) Down-regulating Circular RNA Prkcsb suppresses the inflammatory response after spinal cord injury. *Neural Regen Res* 17:144–151
  44. Wang WZ, Li J, Liu L, Zhang ZD, Li MX, Li Q, Ma HX, Yang H et al (2021) Role of circular RNA expression in the pathological progression after spinal cord injury. *Neural Regen Res* 16:2048–2055
  45. Wang Y, Wang Z (2015) Efficient backsplicing produces translatable circular mRNAs. *RNA (New York, NY)* 21:172–179
  46. Qu S, Yang X, Li X, Wang J, Gao Y, Shang R, Sun W, Dou K et al (2015) Circular RNA: A new star of noncoding RNAs. *Cancer Lett* 365:141–148
  47. Chen LL (2016) The biogenesis and emerging roles of circular RNAs. *Nat Rev Mol Cell Biol* 17:205–211
  48. Li X, Lou X, Xu S, Du J, Wu J (2020) Hypoxia inducible factor-1 (HIF-1 $\alpha$ ) reduced inflammation in spinal cord injury via miR-380-3p/NLRP3 by Circ 0001723. *Biol Res* 53:35
  49. Chen J, Fu B, Bao J, Su R, Zhao H, Liu Z (2021) Novel circular RNA 2960 contributes to secondary damage of spinal cord injury by sponging miRNA-124. *J Comp Neurol* 529:1456–1464
  50. Wang W, He D, Chen J, Zhang Z, Wang S, Jiang Y, Wei J (2021) Correction for: Circular RNA Plek promotes fibrogenic activation by regulating the miR-135b-5p/TGF- $\beta$ R1 axis after spinal cord injury. *Aging* 13:16897
  51. Huang Q, Wang C, Hou Z, Wang G, Lv J, Wang H, Yang J, Zhang Z et al (2017) Serum microRNA-376 family as diagnostic and prognostic markers in human gliomas. *Cancer Biomark* 19:137–144
  52. Li H, Xue Y, Ma J, Shao L, Wang D, Zheng J, Liu X, Yang C et al (2019) SNHG1 promotes malignant biological behaviors of glioma cells via microRNA-154-5p/miR-376b-3p-FOXP2-KDM5B participating positive feedback loop. *J Exp Clin Cancer Res* 38:59
  53. Liu XW, Zhang CC, Zhang T (2020) MiR-376b-3p functions as a tumor suppressor by targeting KLF15 in non-small cell lung cancer. *Eur Rev Med Pharmacol Sci* 24:9480–9486
  54. Liu Y, Liu X, Ye P, Zhang X, Schilling AF, Yonezawa T, Gao G, Cui X (2020) MicroRNA-191 regulates differentiation and migration of mesenchymal stem cells and their paracrine effect on angiogenesis. *Biotechnol Lett* 42:1777–1788
  55. Kobashi S, Terashima T, Katagi M, Nakae Y, Okano J, Suzuki Y, Urushitani M, Kojima H (2020) Transplantation of M2-Deviated Microglia Promotes Recovery of Motor Function after Spinal Cord Injury in Mice. *Mol Ther* 28:254–265
  56. Li X, Luo D, Hou Y, Hou Y, Chen S, Zhan J, Luan J, Wang L et al (2020) Sodium Tanshinone IIA Silate Exerts Microcirculation Protective Effects against Spinal Cord Injury In Vitro and In Vivo. *Oxidative Med Cell Longev* 2020:3949575
  57. Oudega M (2012) Molecular and cellular mechanisms underlying the role of blood vessels in spinal cord injury and repair. *Cell Tissue Res* 349:269–288
  58. DeLisser HM, Christofidou-Solomidou M, Strieter RM, Burdick MD, Robinson CS, Wexler RS, Kerr JS, Garlanda C et al (1997) Involvement of endothelial PECAM-1/CD31 in angiogenesis. *Am J Pathol* 151:671–677
  59. Moss A (2013) The angiopoietin: Tie 2 interaction: a potential target for future therapies in human vascular disease. *Cytokine Growth Factor Rev* 24:579–592

**Publisher's Note** Springer Nature remains neutral with regard to jurisdictional claims in published maps and institutional affiliations.

Springer Nature or its licensor (e.g. a society or other partner) holds exclusive rights to this article under a publishing agreement with the author(s) or other rightsholder(s); author self-archiving of the accepted manuscript version of this article is solely governed by the terms of such publishing agreement and applicable law.